

# Introduction of Physical Transport Mechanisms into 2D Hybrid Hall Thruster Simulations

Michelle K. Allis,<sup>\*</sup> Cliff A. Thomas,<sup>\*</sup> Nicolas Gascon,<sup>†</sup> and Mark A. Cappelli<sup>‡</sup>

*Stanford University, Stanford, CA, 94305*

Eduardo Fernandez<sup>§</sup>

*Eckerd College, St. Petersburg, FL, 33711*

A limitation of many currently existing Hall thruster models is the need for an ad-hoc or experimentally-based electron cross field mobility. In this work, the potential fluctuations simulated using a radial-axial hybrid Hall thruster model are used to calculate a new electron mobility based only on simulated properties. A small amplitude perturbation model is used to compute number density and electron velocity fluctuations and to develop a linearized dispersion relation based on a two-stream instability. The simplified dispersion relation is used to infer azimuthal wave behavior from the simulated axial properties. The correlation between the relative phase of the plasma density and electron velocity are used to compute anomalous contributions to axial and azimuthal current density. The computed Hall parameter based on this approach leads to improved agreement between simulation and experimental measurements of plasma properties. However, for the specific thruster modelled, the simulated perturbation quantities are not small as originally assumed. While this decreases the validity of the computed mobility, it shows that fluctuations likely play a significant role in transport and emphasizes the need for a self-consistent non-linear model.

## Nomenclature

$\vec{B}$	Magnetic Field, T
$\vec{E}$	Electric Field, V/m
$e$	Electron Charge, C
$J$	Current Density, A/m <sup>2</sup>
$\vec{k}$	Perturbation Wavenumber, 1/m
$m$	Mass, kg
$n$	Number Density, m <sup>-3</sup>
$q$	Charge, C
$U$	Velocity, m/s
$\phi$	Electric Potential, V
$\mu$	Mobility, m <sup>2</sup> /Vs
$\omega$	Perturbation Frequency, rad/s
$\omega_p$	Plasma Frequency, rad/s
$\Omega$	Cyclotron Frequency, rad/s
$\omega\tau$	Hall Parameter

### Subscript

$e$	Electron
$i$	Ion

<sup>\*</sup>Research Assistant, Mechanical Engineering Department, Building 520. Student Member, AIAA.

<sup>†</sup>Research Associate, Mechanical Engineering Department, Building 520, Member, AIAA.

<sup>‡</sup>Professor, Mechanical Engineering Department, Building 520, Member, AIAA.

<sup>§</sup>Associate Professor, Physics Department.

$o$	Time-Average
$\theta$	Azimuthal Direction
$z$	Axial Direction

## I. Introduction

DUE to their high efficiency, low mass, and large specific impulse, Hall thrusters<sup>1</sup> are ideal devices for both satellite station keeping and missions to the outer planets. However, although Hall thrusters have been successfully employed in space applications for decades, optimization of these devices cannot occur until all of the physics governing operation are well-understood. Presently, simulations exist which can reproduce experimental measurements with reasonable accuracy.<sup>2-5</sup> This suggests that most of the fundamental governing principles behind Hall thruster operation are understood and successfully captured. However, most numerical models include simplifications in the description of certain phenomena, such as cross field electron transport, which bypass the need for fundamental understanding and make modelling of new thrusters difficult.

Experimental observations have shown that electrons cross magnetic field lines faster than classically predicted based on their collision rate with neutral particles. Sources of this anomalous transport have been attributed to electron collisions with channel walls and turbulence in the plasma. However, despite a basic understanding of the cause of the anomalous mobility, implementation of this understanding in simulations typically involves thruster-specific parameters which are adjusted to provide the best agreement with experiment. Another method used to describe cross field transport is an implementation of an experimentally determined electron mobility.<sup>6</sup> While both of these methods give satisfying results for the specific thruster modelled, they cannot be used to predict the plasma properties and performance of newly designed thrusters.

Therefore, the goal of this research is to implement a 2D (radial-axial) hybrid particle-in-cell (PIC) numerical simulation in which the mobility is calculated based on simulated plasma properties using the experimental mobility as the starting condition. The simplified model used to compute mobility is a linearized small perturbation model based on the observed frequencies and axial wavenumbers of fluctuations in the simulation. A simple dispersion relation is used to calculate both the azimuthal wavenumbers and imaginary components of the wave vectors which cannot be directly captured in the radial-axial simulation. These fluctuations are used to calculate perturbations of the time-averaged electron velocities and number densities which are then used to calculate anomalous currents in both the axial and azimuthal directions. Preliminary results have been successful at capturing experimentally observed phenomena, underscoring the importance of fluctuations in describing transport. However, the substantial size of the perturbation quantities calculated using the linearized model is inconsistent with the small amplitude assumption, suggesting that an improved non-linear model may eventually be required in order to achieve self-consistency.

## II. Linearized Small Perturbation Model

The main premise behind the proposed model for anomalous cross field mobility is that electron-ion streaming instabilities in a Hall thruster cause fluctuations in electric potential. These potential fluctuations produce correlated perturbations in the electron velocity and number density, leading to enhanced transport. Since the PIC code does not directly capture the relative phase of the plasma density and velocity fluctuations, the effect of these instabilities is input into the simulation using a constant, spatially-varying Hall parameter.

$$\omega\tau = \frac{\langle J_{e\theta} \rangle}{\langle J_{ez} \rangle} \quad (1)$$

where both the time-averaged azimuthal current density,  $\langle J_{e\theta} \rangle$ , and axial current density,  $\langle J_{ez} \rangle$ , consist of a base term, based on time-averaged quantities, and an anomalous term, based on perturbation quantities.

$$\langle J_{e(\theta,z)} \rangle = \langle J_{e(\theta,z)} \rangle_{base} + \langle J_{e(\theta,z)} \rangle_{anom} \quad (2)$$

Once this Hall parameter is calculated using the anomalous contributions to current density, the electron cross field mobility is assumed to be:

$$\mu_{e\perp} = \frac{1}{\omega\tau B} \quad (3)$$

In order to calculate the anomalous current density, we first assume that the electron velocity,  $\vec{U}_e$ , ion velocity,  $\vec{U}_i$ , electron density,  $n_e$ , ion density,  $n_i$ , and electric potential,  $\phi$ , exhibit small amplitude planar fluctuations on top of their time-averaged values. Therefore, we assume these quantities can be expressed in the form:

$$f = f_o + \tilde{f} \exp \left( i(\vec{k} \cdot \vec{r} - \omega t) \right) \quad (4)$$

where  $\omega$  is a real-valued quantity and  $\vec{k}$  is a complex vector in the  $z - \theta$  plane. In the following analysis, products of small amplitude complex perturbations,  $\tilde{f}$ , are neglected, and time averaged quantities,  $f_o$ , are assumed to be spatially uniform. Also, cylindrical effects are ignored and the directions,  $\hat{\theta}$ ,  $\hat{z}$ , and  $\hat{r}$  are assumed to be rectilinear.

Substituting these perturbation values into the electron and ion continuity equations, neglecting production, yields an expression for the electron and ion density perturbation magnitude.

$$\tilde{n}_{(e,i)} = \frac{\vec{k} \cdot \vec{U}_{(e,i)}}{\omega - \vec{k} \cdot \vec{U}_{(e,i),o}} n_{(e,i),o} \quad (5)$$

In the electron and ion momentum equations, the pressure and collisional forces are neglected, and the magnetic field is assumed to be entirely in the radial direction. Linearizing these equations yields expressions for the electron and ion perturbation velocities in the azimuthal and axial directions.

$$\tilde{U}_{(e,i),z} = \frac{q_{(e,i)}}{m_{(e,i)}} \frac{1}{(\omega_{(e,i)}^2 - \Omega_{(e,i)}^2)} \left( \omega_{(e,i)} \tilde{\phi} k_z + \Omega_{(e,i)} \tilde{\phi} k_\theta \right) \quad (6)$$

$$\tilde{U}_{(e,i),\theta} = \frac{q_{(e,i)}}{m_{(e,i)}} \frac{1}{(\omega_{(e,i)}^2 - \Omega_{(e,i)}^2)} \left( -i\Omega_{(e,i)} \tilde{\phi} k_z + \omega_{(e,i)} \tilde{\phi} k_\theta \right) \quad (7)$$

where  $\omega_{(e,i)} = \omega - \vec{k} \cdot \vec{U}_{(e,i),o}$ . Substituting Eqs. (6) and (7) into Eq. (5) yields a simplified expression for the number density perturbation.

$$\tilde{n}_{(e,i)} = \frac{q_{(e,i)}}{m_{(e,i)}} \left( \frac{k^2}{\omega_{(e,i)}^2 - \Omega_{(e,i)}^2} \right) \tilde{\phi} n_{(e,i),o} \quad (8)$$

In order to relate the frequency,  $\omega$ , and the complex wave vector,  $\vec{k}$ , a dispersion relation<sup>7</sup> is calculated using Poisson's equation:

$$\nabla^2 \phi = - \frac{e(n_i - n_e)}{\epsilon_o} \quad (9)$$

Combining Eqs. (8) and (9) yields:

$$1 = \frac{\omega_{p,i}^2}{(\omega - \vec{k} \cdot \vec{U}_{i,o})^2 - \Omega_i^2} + \frac{\omega_{p,e}^2}{(\omega - \vec{k} \cdot \vec{U}_{e,o})^2 - \Omega_e^2} \quad (10)$$

Once the relationship between  $\vec{k}$  and  $\omega$  is established, the perturbation in electron number density and electron velocity in the azimuthal and axial directions can be determined using Eqs. (6)-(8). With these quantities, the anomalous contributions to current density can be calculated.

$$\langle J_{e,(\theta,z)} \rangle_{anom} = \left\langle q_e \text{Re}[\tilde{n}_e] \text{Re}[\tilde{U}_{e,(\theta,z)}] \right\rangle \quad (11)$$

where  $\text{Re}[\tilde{f}]$  indicates the real component of the complex quantity,  $\tilde{f}$ . Averaging over a period,  $\frac{\omega}{2\pi}$ , yields:

$$\langle J_{e,(\theta,z)} \rangle_{anom} = \frac{1}{2} \text{Re} \left[ q_e \tilde{n}_e \tilde{U}_{e,(\theta,z)}^* \right] \quad (12)$$

where \* indicates the complex conjugate. By summing the anomalous contribution to current density with the classical, base current, the Hall parameter can be calculated using Eq. (15). For more details on the numerical implementation see Sec. III-B.

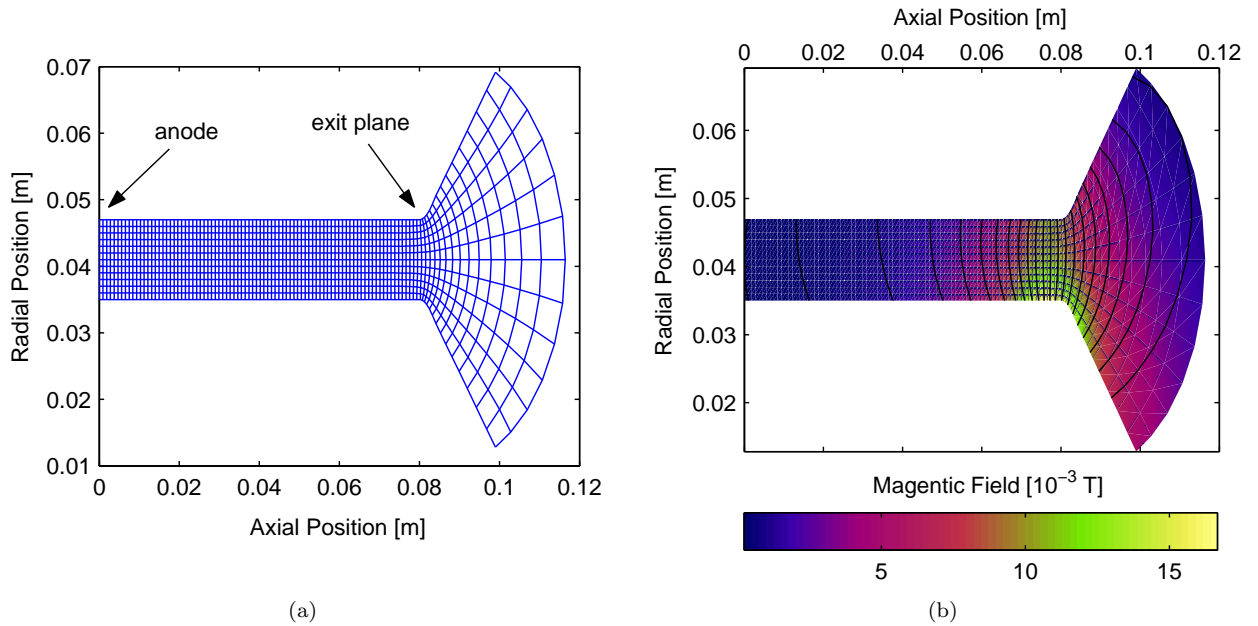


Figure 1. 1(a) Computational grid of the Stanford Hall Thruster radial-axial simulation. 1(b) Magnetic field strength and contour lines of the Stanford Hall Thruster.

### III. Numerical Model

#### A. Hybrid PIC Simulation

The numerical simulation used to both calculate and implement a new electron mobility is a radial-axial hybrid PIC model<sup>8</sup> based on work by Fife.<sup>9</sup> The model employs a quasi-one-dimensional fluid treatment of electrons and a 3-D particle-in-cell (PIC) treatment of the heavy species, Xe and Xe<sup>+</sup>. The two solutions are coupled assuming space-charge neutrality.

The computational geometry used in the simulation corresponds to the laboratory discharge referred to here as the Stanford Hall Thruster. The annular channel is approximately 8 cm in length and 1.2 cm in width. The computational grid, which includes a 2-D slice of the channel and near field region, is shown in Fig. 1(a). The insulating channel walls are made of alumina. A mass flow rate of 2 mg/s is implemented in the model to match experimental conditions. Measurements of the magnetic strength in the radial and axial directions along the channel centerline are used to impose a constant external magnetic field as shown in Fig. 1(b). Only a discharge voltage of 200 V is considered in the results presented.

The electron fluid is governed by a continuity equation, momentum equations parallel and perpendicular to the magnetic field, a 1D electron energy equation, and a current continuity equation. An electron mobility is assumed in order to calculate the electron cross field velocity and thermal diffusivity. The electron mobility along magnetic field lines is assumed to be infinite resulting in isothermal magnetic field contours. However, the pressure gradient contribution to electric potential in the parallel direction is included. The electron energy equation includes a joule heating energy source term and ionization and wall damping energy sink terms. The wall damping treatment is similar to that of Barral *et al.*<sup>10</sup> However, while Barral calculates a separate temperature parallel to magnetic contours in order to determine heat transfer, this model lowers the effective temperature at the wall to account for anisotropy and the non-Maxwellian nature of the velocity distribution function. The effective temperature producing the best agreement with experiment was found to be 40% of the perpendicular temperature.

The motion of the heavy particles species, Xe and Xe<sup>+</sup>, is solved in three dimensions using cylindrical coordinates. Neutral particles are injected at the anode and scatter off channel walls assuming a one way Maxwellian flux distribution. Ions which impact channel walls are neutralized before being re-emitted into the channel. Ionization and charge exchange collisions take place everywhere inside the computational domain based on local plasma properties. Neutral particles are injected from the computational boundaries

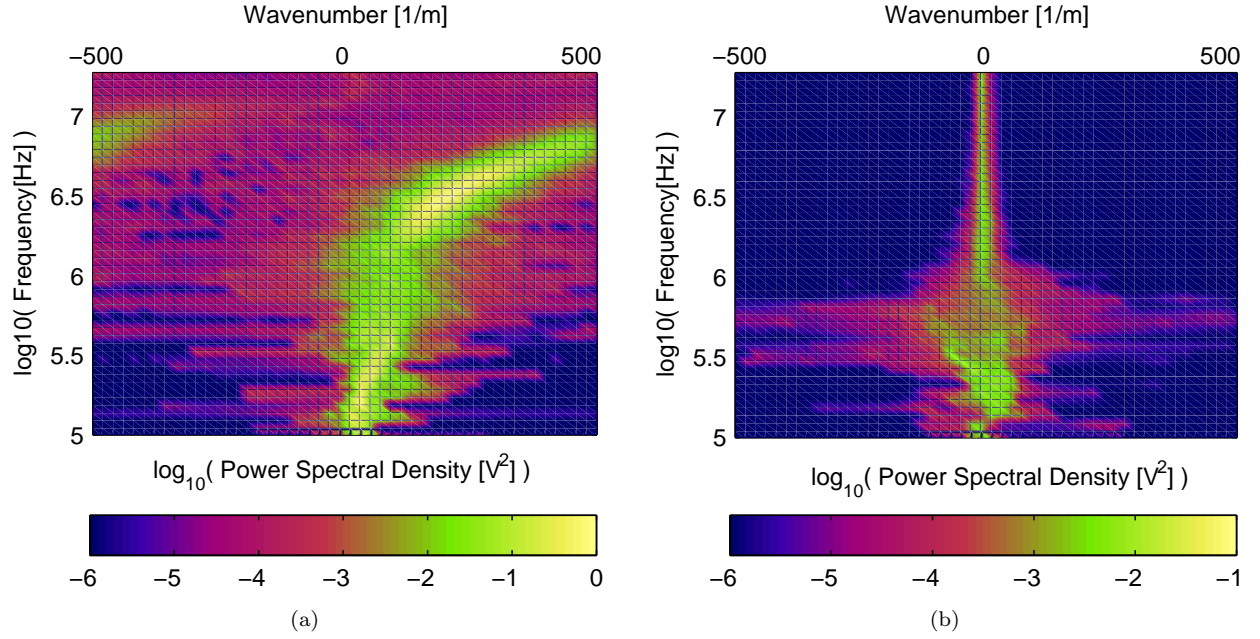


Figure 2. 2(a) Real component of axial wavenumber vs. frequency along centerline 5 mm upstream of exit plane. 2(b) Real component of axial wavenumber vs. frequency along centerline 4 cm upstream of exit plane.

in the near-field region in order to simulate a back pressure of 0.05 mTorr.

For computational manageability, superparticles are used to represent large groups of neutrals and ions rather than simulating individual particles. Since neutral and ion densities differ by orders of magnitude over the length of the domain, the size of the superparticles vary with both space and species. The simulation is initialized with approximately 400,000 superparticles of each heavy particle species. The ion and neutral time step is typically 25 ns, while the electron time step is 0.1 ns. On a 3.8 GHz Pentium 4 processor, the simulation completes 625  $\mu$ s in one day.

## B. Mobility Implementation

Like many numerical methods, a shortcoming of this approach is that it requires an initial assumption of the solution before an updated solution can be calculated. An initial guess of the mobility is necessary in order to simulate the plasma properties which will be used to calculate the updated mobility. For our simulation, the initial Hall parameter was determined using the experimental profile calculated by Meezan *et al.*<sup>6</sup> Since experimental measurements only exist along the centerline, the initial mobility was assumed to be radially uniform. Also, since the measured profile did not extend to the edges of the computational domain, the mobility for regions beyond the measurements was taken to be equal to the nearest measured mobility.

Using the experimental mobility, plasma properties are simulated over approximately one breathing mode and used to calculate the stationary state of the azimuthal and axial current densities. The radial magnetic field and time-averaged axial electric field are used to calculate the base azimuthal current density resulting from time-averaged quantities. In addition, the time-averaged plasma density, neutral density, and electron temperature are used to calculate the electron-neutral collision frequency at each time step. The electron momentum exchange collision cross section is obtained from the Siglo database (<http://www.siglo-kinema.com/database>). The base current density in the axial direction is calculated using the time-averaged collision and cyclotron frequency.

$$\langle J_{e,\theta} \rangle_{base} = \frac{\langle E_z \rangle}{B_r} \quad (13)$$

$$\langle J_{e,z} \rangle_{base} = \frac{\langle \nu_{en} \rangle}{\Omega_e} \frac{\langle E_z \rangle}{B_r} \quad (14)$$

To calculate the fluctuating perturbation quantities in Eqs. (6)-(8), a wavelet analysis is performed on the spatially-varying, transient, simulated potential data. A wavelet analysis was chosen over a simple Fourier decomposition to reduce the sensitivity of results to transients and edge effects, and improve the signal to noise statistics. Morlet wavelets are used to decompose the potential results to find the power spectral density at each frequency and real component of axial wavenumber. At each position, the frequency and wavenumber corresponding to the largest power spectral density are assumed to represent the dominant mode observed at that location. The maximum power spectral density is then used to calculate the simulated potential fluctuation for that mode. While the assumption of one dominant mode is reasonable in certain locations of the Hall thruster, such as in the region of strong electric field, upstream of the ionization zone the wavenumber and frequency are not well-defined, leading to a somewhat arbitrary choice of frequency and axial wavenumber. The dispersion relation at two positions along the centerline of the thruster are shown in Fig. 2. Note that a numerical artifact of the wavelet analysis produces aliasing at low wavenumbers, as shown in Fig. 2(a). This process of examining the dispersion relation to determine a frequency, real component of axial wavenumber, and potential fluctuation amplitude is repeated for each cell of the computational grid.

Once the frequency and real component of axial wavenumber are determined, the dispersion relation, Eq. (10), is used to calculate the magnitude and direction of the complex wavenumber. One complexity associated with this method is that for each simulated axial wavenumber and frequency either zero or 16 solutions for the complex wavenumber exist.

For approximately half of the simulated positions inside the channel, not localized to any specific region, the simulated results simply cannot satisfy the dispersion relation. When this happens, the calculation at these locations is terminated and a mobility is deduced through interpolation from nearby points. For the other half of the cells, 4 distinct complex wavenumbers, each with 4 possible directions, satisfy the observed frequency and real component of axial wavenumber. Of these 16 solutions, 4 correspond to growing waves, 4 to decaying waves, and 8 have no imaginary component of wavenumber. Four of the waves are in each of the four possible quadrant directions in the azimuthal-axial plane. Half of the solutions correspond to quasineutral perturbations; the other half have differing ion and electron perturbation magnitudes and phases. If experimental data existed to indicate which direction the waves were travelling, choosing an appropriate root would be more straightforward. For this model, only one root increases transport everywhere and corresponds to a growing instability. This will be the only root considered and discussed. Note that this root corresponds to a wave with quasineutral perturbations and is primarily azimuthal in the negative  $\vec{E} \times \vec{B}$  direction. In the last centimeter of the channel, this wave has an axial component nearly equal to the azimuthal component in the negative  $\hat{z}$  direction, toward the anode.

Given the complex azimuthal and axial complex wavenumbers, as well as the frequency, simulated potential fluctuation magnitude, and time-averaged quantities, the perturbations in number density and velocity can be calculated and substituted into Eq. (12) to calculate the anomalous current density in the azimuthal and axial directions.

The Hall parameter is then simply calculated at each position in the radial axial plane using:

$$\omega\tau = \frac{\langle J_{e,\theta} \rangle_{base} + \langle J_{e,\theta} \rangle_{anom}}{\langle J_{e,z} \rangle_{base} + \langle J_{e,z} \rangle_{anom}} \quad (15)$$

Note that any Hall parameter which is calculated to be negative is discarded, since the code becomes numerically unstable if the electron current reverses direction. Also, outside the channel where the grid and contour spacing is large, this analysis does not yield consistent results from point to point. Therefore, beyond the exit plane, the experimental mobility is retained.

The two-dimensional computed Hall parameter is then input into the simulation, and the process is repeated. Ideally, the solution would converge such that the input Hall parameter produced fluctuations consistent with the fluctuations used to compute the Hall parameter. However, due to the sensitivity of the simulation to small changes in the mobility as well as simulated fluctuations which violate the small amplitude assumption, convergence has not yet been obtained.

## IV. Results and Discussion

Using the simulated results calculated using the experimental mobility, a new mobility was computed using the method described in Sec. III-B. Fig. 3 shows that this first iteration captures the increase in transport that occurs throughout the entire channel. The classical inverse Hall parameter is calculated using

the time averaged electron neutral collision rate. Also shown in Fig. 3, the location and magnitude of the calculated minimum in the inverse Hall parameter is in good agreement with experimental measurements.

Fig. 4 shows the two-dimensional nature of the calculated transport coefficient. After inputting this computed Hall parameter into the numerical model, the simulation was run again for approximately 10 breathing mode cycles. The time averaged results of electron temperature and electric potential are shown in Fig. 5. As illustrated in these figures, for most plasma properties the computed mobility does a better job at reproducing experimental measurements<sup>11,12</sup> than the experimentally-based mobility. Note that the experimental mobility contains a significant amount of experimental uncertainty. In Fig. 5(a), the simulated electron temperature profile using the calculated mobility is broader than that simulated using the experimental mobility. This broadening results in a more gradual potential drop, which is also in better agreement with observations. Due to the improvement in simulated electric field, the ions no longer exhibit a strong backflow region near the anode, as shown in Fig. 5(b).

The widening of the electron temperature also causes an improvement in the simulated plasma potential. Using the computed mobility, the peak in plasma density is  $9.8 \times 10^{17} \text{m}^{-3}$  compared with the experimentally measured value of  $9.2 \times 10^{17} \text{m}^{-3}$ . Using the experimental mobility, the peak in plasma density is only  $6.4 \times 10^{17} \text{m}^{-3}$ . Also, due to the slight increase in mobility over the majority of the channel, the total anode current increases from 1.7 A using the experimental Hall parameter to 2.5 A using the computed Hall parameter. The experimentally measured anode current at a discharge voltage of 200 V is 2.7 A.

Despite the surprising success of the first iteration, a few issues possibly make the improvement more fortuitous than legitimate. First, while successive iterations are still overall better at reproducing the experimental results than the experimental mobility, they generally are not quite as good as the first iteration, and do not seem to be converging to a constant time-averaged mobility. However, this is expected since the assumptions used in deriving the model are inconsistent with the model results, as discussed in more detail below. Second, as previously mentioned, the choice of which root to pick in the solution of the dispersion relation is somewhat arbitrary. While many of the roots produce similar computed mobilities, there presently is no way to tell which of these roots, if any, is dominant. It is possible that several roots may contribute to transport in various degrees throughout the channel.

The biggest issue with the model in its present form, however, is that the computed number density and electron velocity perturbations are several times larger than their simulated time-averaged counterparts for the majority of the channel. In the most severe case, for a few isolated locations, the computed electron number density perturbation is ap-

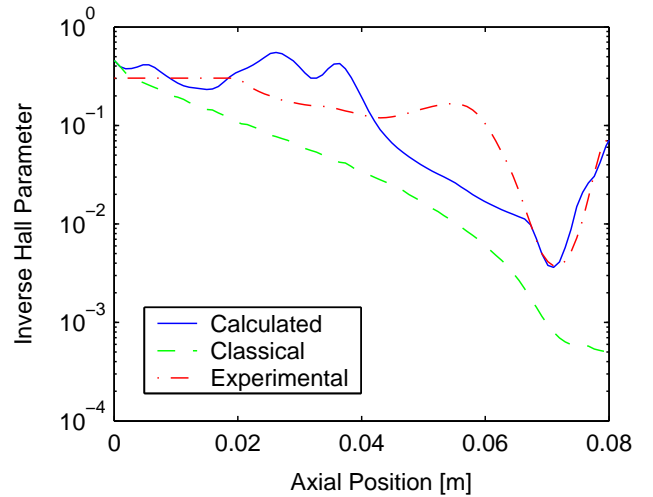


Figure 3. Computed, classical, and experimentally determined inverse Hall parameters along the centerline of the Stanford Hall Thruster.

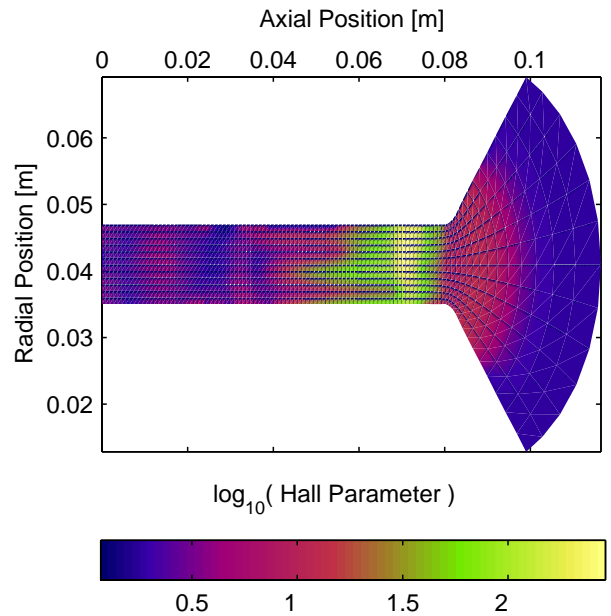
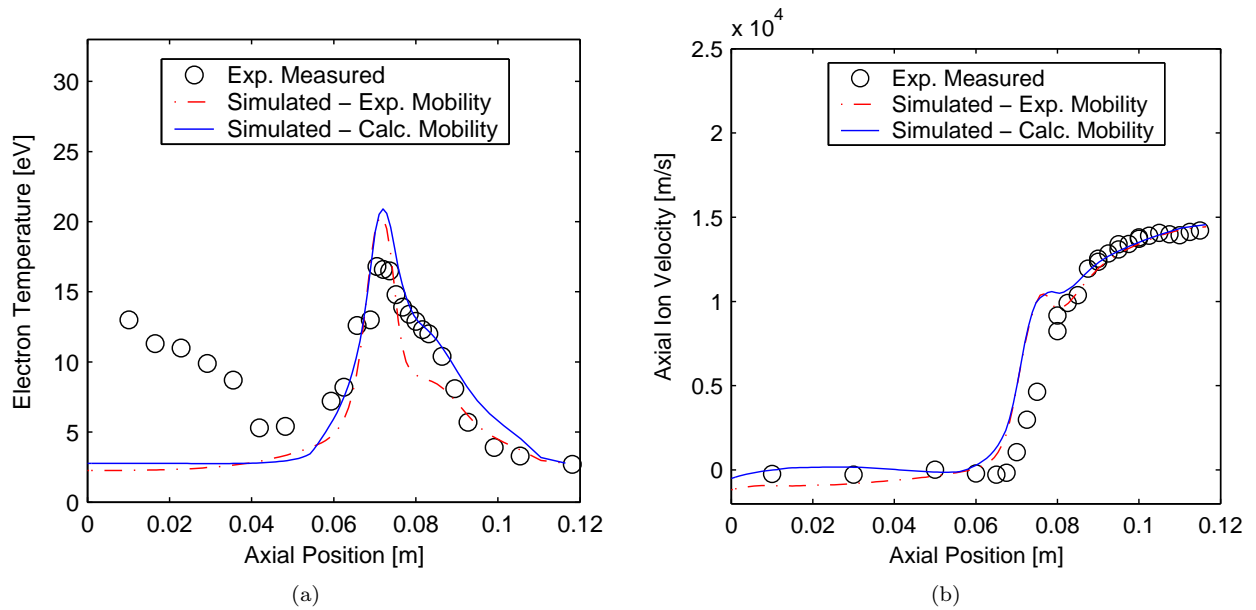


Figure 4. Computed 2D Hall parameter over the computational domain of the simulation.



**Figure 5.** 5(a) Comparison of simulated electron temperature with experimental measurements using the experimental mobility and the calculated mobility. 5(b) Comparison of simulated electron temperature with experimental measurements using the experimental mobility and the calculated mobility.

proximately 100 times larger than the time averaged quantity. While this invalidates the small amplitude assumption used to compute the dispersion relation and perturbation magnitudes, the verification of this invalidation is noteworthy. Although the perturbation quantities are not being calculated correctly due to the invalid assumption, the inadequacy of the small amplitude model suggests that fluctuations are in fact non-negligible and may likely play a dominant role in transport.

## V. Summary

A simplified linear perturbation model has been employed to calculate and implement a new electron cross field mobility in a 2D hybrid Hall thruster simulation. The model uses the simulated potential fluctuations computed using an experimental mobility and a linearized dispersion relation to extract information about azimuthal behavior. Combining this information with time-averaged simulated quantities, perturbations in number density and electron velocity are computed. The correlation between the relative phase of these fluctuating quantities produces an anomalous current density which enhances axial electron transport. The fact that the fluctuation magnitudes exceed the limitations of the quasi-linear model shows that the perturbations are not small as originally assumed, reinforcing the idea that fluctuations are a likely cause of transport, and validating the need for a nonlinear model.

Despite the limitations of the small amplitude linear model, results have shown that a computed mobility based on simulated fluctuations can be used to describe transport and, in many cases, better predict experimental measurements than an experimental mobility. However, in the future, the assumption of small amplitude perturbations must be relaxed to account for the possibility of instabilities which produce large variations in plasma properties.

## Acknowledgments

This research was supported by the Air Force Office of Scientific Research. Stipend support for M.S. was provided through a fellowship from the National Science Foundation. N.G. was partially supported by a fellowship from the European Space Agency. E.F. acknowledges the Center for Turbulent Research for supporting this work and K. Mahesh for valuable assistance in the early stages of code development. M.C. and N.G. would like to thank Caroline Vialard-Goudou for her contribution to improving the electron

diffusion description in the code.

## References

- <sup>1</sup>Zhurin, V., Kaufman, H., and Robinson, R., "Physics of closed drift thrusters," *Plasma Sources Science and Technology*, Vol. 8, 1999.
- <sup>2</sup>Bareilles, J., Hagelaar, G., Garrigues, L., Boniface, C., Boeuf, J., and Gascon, N., "Critical assessment of a two-dimensional hybrid Hall thruster model: Comparisons with experiment," *Physics of Plasmas*, Vol. 11, No. 6, 2003, pp. 3035.
- <sup>3</sup>Ahedo, E., Martínez-Cerezo, P., and Sánchez, M. M., "One-dimensional model of the plasma flow in a Hall thruster," *Physics of Plasmas*, Vol. 8, No. 6, 2001.
- <sup>4</sup>Keidar, M., Boyd, I., and Beilis, I., "Plasma flow and plasma-wall transition in Hall thruster channel," *Physics of Plasmas*, Vol. 8, No. 12, 2001.
- <sup>5</sup>Allis, M., Gascon, N., Cappelli, M., and Fernandez, E., "Effect of Charge Exchange on 2D Hall Thruster Simulation," *Proceedings of the 29th International Electric Propulsion Conference*, 2005.
- <sup>6</sup>Meezan, N., Hargus, W., and Cappelli, M., "Anomalous electron mobility in a coaxial hall plasma discharge," *Physical Review E*, Vol. 63, No. 026420, 2001.
- <sup>7</sup>Guerrini, G. and Michaut, C., "Characterization of high frequency oscillations in a small Hall-type thruster," *Physics of Plasmas*, Vol. 6, No. 1, 1999.
- <sup>8</sup>Fernandez, E., Cappelli, M., and Mahesh, K., "2D simulations of hall thrusters," *CTR Annual Research Briefs*, 1998, pp. 81.
- <sup>9</sup>Fife, J., *Nonlinear hybrid-PIC modeling and electrostatic probe survey of hall thrusters*, Ph.D. thesis, Massachusetts Institute of Technology, 1998.
- <sup>10</sup>Barral, S., Makowski, K., Peradzynski, Z., Gascon, N., and Dudeck, M., "Wall material effects in stationary plasma thrusters II: Near wall and inner-wall conductivity," *Physics of Plasmas*, Vol. 10, No. 10, 2003.
- <sup>11</sup>Hargus, W., *Investigation of the plasma acceleration mechanism within a coaxial Hall thruster*, Ph.D. thesis, Stanford University, 2001.
- <sup>12</sup>Cedolin, R., *Laser-induced fluorescence diagnostics of xenon plasmas*, Ph.D. thesis, Stanford University, 1997.